Supporting Information for "Relation of the double-ITCZ bias to the atmospheric energy budget in climate models"

Ori Adam[1], Tapio Schneider[1,2], Florent Brient[1], and Tobias Bischoff[2]

Contents of this file

1. First- and third-order approximations of the energy flux equator
2. Figures S1 to S2
3. Table S1

Introduction Here we describe approximate solutions of the energy flux equator (EFE), which provide a basis for relating cross-equatorial atmospheric energy transport AET_0 and equatorial net energy input NEI_0 to hemispherically symmetric and antisymmetric variations in the zonal-mean tropical precipitation. We also discuss the sensitivity of AET_0 and NEI_0, and of the tropical precipitation indices A_P and E_P, to the meridional averaging

[1]Department of Earth Sciences, ETH

Zürich, 8092 Zürich Switzerland

[2]California Institute of Technology,

Pasadena, CA, USA

boundaries. The values of the tropical precipitation indices for 31 models participating in the Coupled Model Intercomparison Project phase 5 (CMIP5) used in the analysis are provided in Table S1.

First- and third-order approximations of the energy flux equator

The first- and third-order approximations of the zonal-mean energy flux equator (EFE) are described in *Bischoff and Schneider* [2014] and *Bischoff and Schneider* [2016]. A review of the underlying concepts can be found in *Schneider et al.* [2014].

Neglecting annual-mean energy storage by the atmosphere, the annual- and zonal-mean column-integrated energy balance of the atmosphere can be written as [*Bischoff and Schneider*, 2014]

$$\frac{1}{a\cos(\phi)}\partial_\phi\Big(\langle vh\rangle\cos(\phi)\Big) = \mathrm{NEI}\ . \tag{1}$$

On the lhs, angle brackets $\langle\cdot\rangle$ denote the mass weighted column integral, h denotes moist static energy (MSE, the sum of the enthalpy, potential energy, and latent energy of the atmosphere), and v is the meridional wind. The rhs is the atmospheric net energy input (NEI), composed of the difference of top of the atmosphere (TOA) net radiative input and surface heat uptake (associated primarily with ocean heat storage or transport).

Assuming the EFE and ITCZ are collocated, the atmospheric energy transport (AET) must vanish at the ITCZ. By expanding $\langle vh\rangle$ at the equator to first order, assuming it vanishes at the ITCZ at latitude ϕ_I, and using Eq. (1), we obtain

$$\phi_I = -\frac{\langle vh\rangle_0}{(\partial_\phi\langle vh\rangle)_0} = -\frac{1}{a}\frac{\mathrm{AET}_0}{\mathrm{NEI}_0}, \tag{2}$$

where $(\cdot)_0$ denotes an equatorial average.

A single ITCZ (and therefore single EFE) is associated with the rising branch of a tropical meridional overturning circulation transporting energy away from the ITCZ. Thus, since the AET is positive north of the ITCZ and negative south of the ITCZ, the meridional gradient of the AET (i.e., approximately the NEI) near a single ITCZ is positive (Fig. S1a).

Since $\langle vh \rangle$ generally increases in the tropics, a negative NEI_0 implies a nonlinear AET distribution there. For sufficiently negative NEI_0, AET will have 3 roots. Such a distribution corresponds to a double-ITCZ state, in which AET vanishes at the ITCZ on either side of the equator, and at the divider between the ITCZs [Fig. S1b; *Bischoff and Schneider*, 2016].

On Earth, the zonal-mean NEI_0 is positive. However, NEI_0 is generally negative in the eastern Pacific [*Bischoff and Schneider*, 2016] where double-ITCZ states occur during boreal spring [*Zhang*, 2001; *Gu et al.*, 2005]. Similarly, increased occurrence of double-ITCZ states is observed in the eastern Pacific during La Niña conditions [*Zhang*, 2001; *Gu et al.*, 2005], which are associated with reduced NEI_0 due to increased ocean heat uptake [*Schneider et al.*, 2014; *Bischoff and Schneider*, 2016]. Thus, in accordance with the EFE framework, reduced NEI in the Pacific sector is consistent with increased occurrence of double-ITCZ states. Therefore, zonally and annually averaged, a decrease in NEI_0 is related to a strengthening of the double-ITCZ signal in the distribution of the tropical precipitation.

Due to increased ocean heat uptake in the eastern-Pacific cold tongue, the zonal-mean NEI_0 decreases sharply near the equator. The sharp variation in the zonal-mean NEI near

the equator renders NEI_0 sensitive to the meridional boundaries of the equatorial average. Figure S2 shows the relation of A_P and AET_0, and the relation of E_P and NEI_0, as in Fig. 2 but with $(\cdot)_0$ corresponding to an average between 2°S and 2°N (compared with 5°S–5°N in Fig. 2). (Note that as CMIP5 AET_0 is calculated from the inter-hemispheric difference in NEI, the model AET_0 values shown in Fig. 2 and Fig. S2 are the same.) It is evident that NEI_0 values are lower in Fig. S2b. However, as in Fig. 2, the ensemble mean NEI_0 is lower than the observed NEI_0, and variations in E_P are positively correlated with variations in NEI_0 ($R = 0.69$ in Fig. S2b vs. $R = 0.66$ in Fig. 2). Thus, while NEI_0 is sensitive to the meridional boundaries of the equatorial average, our results (i.e., the relative variations) are not qualitatively affected by this sensitivity.

Similarly, the results are not qualitatively sensitive to the meridional boundaries of the tropical region used in calculating the tropical asymmetry precipitation index A_P (Eq. 2 of the main text) and the equatorial precipitation index E_P (Eq. 3 of the main text), if the tropical region is defined as equatorward of $\sim 10°$–$20°$. Table S1 provides the values of A_P and E_P for the 31 CMIP5 models used in the analysis.

For either very high or vanishing equatorial precipitation values, E_P becomes insensitive to symmetric variations in the zonal-mean precipitation. However, in the present climate, typical equatorial zonal-mean precipitation values neither vanish nor are much higher than the tropical mean (Fig. 1a); the use of E_P is therefore justified in the present analysis.

References

Bischoff, T., and T. Schneider (2014), Energetic constraints on the position of the Intertropical Convergence Zone, *J. Clim.*, *27* (13), 4937–4951, doi:10.1175/JCLI-D-13-

00650.1

Bischoff, T., and T. Schneider (2016), The equatorial energy balance, ITCZ position, and double ITCZ bifurcations, *J. Clim.*, *29* (8), 2997–3013, doi:10.1175/JCLI-D-15-0328.1

Schneider, T., T. Bischoff, and G.H. Haug (2014), Migrations and dynamics of the intertropical convergence zone, *Nature*, *513*, 45–53, doi:10.1038/nature13636

Gu, G., R. Adler, and A. Sobel (2005), The eastern Pacific ITCZ during the boreal spring, *J. Atmos. Sci.*, **62**, 1157–1174.

Zhang, C., (2001), Double ITCZs, *J. Geophys. Res.*, **106**, 785–11 792.

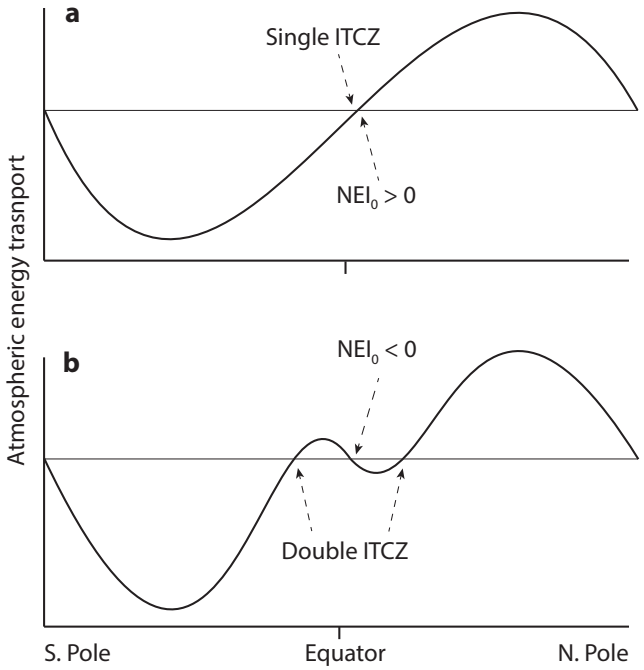

Figure S1. Sketch of column-integrated meridional atmospheric energy transport (AET) in (**a**) single- and (**b**) double-ITCZ states. Equatorial net energy input (NEI_0) is equal to the derivative of the AET at the equator. ITCZs are located where the AET vanishes and diverges.

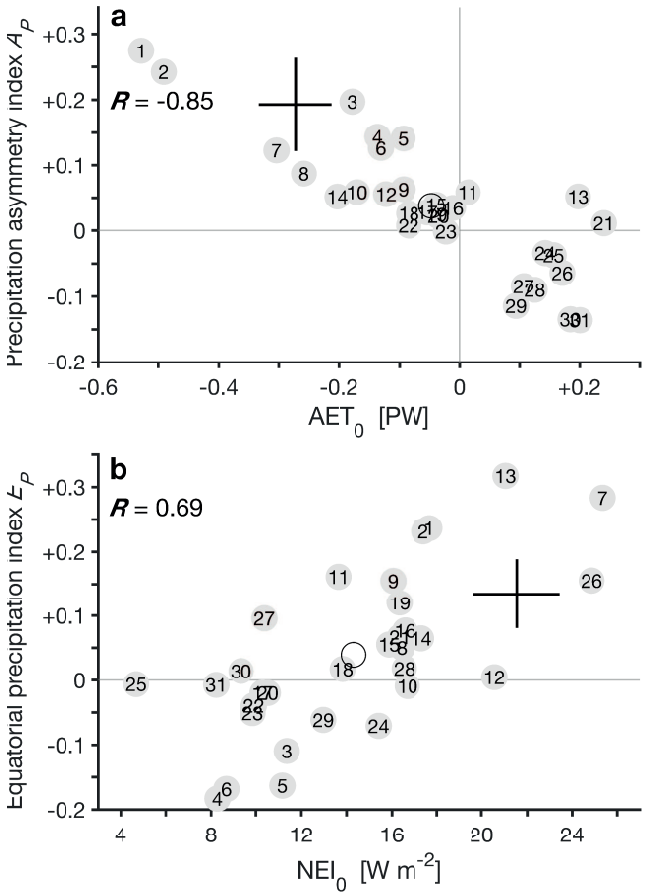

Figure S2. (**a**) Relation of the annual-mean tropical precipitation asymmetry index A_P and cross-equatorial atmospheric energy transport AET_0. (**b**) Relation of the annual-mean equatorial precipitation index E_P and the equatorial atmospheric net energy input NEI_0. CMIP5 models are numbered from largest to smallest A_P (Table S1). Ensemble means are shown in circles, and the observed values (ERAI for energetic quantities and GPCP for precipitation) are shown as bars, whose length corresponds to one standard deviation of interannual variations. ERAI AET_0 and all NEI_0 values are averaged between 2°S and 2°N.

Table S1. ERAI and CMIP5 model names and affiliations, and their climatological (1979-2004) annual- and zonal-mean values of the tropical asymmetry precipitation index A_P, equatorial precipitation index E_P, cross-equatorial atmospheric energy trasnport AET_0, and equatorial atmospheric net energy input NEI_0. Models are ordered from largest to smallest A_P.

	Model	**Affiliation**	A_P	AET_0	E_P	NEI_0
1	MIROC-ESM	JAMSTEC, AORI, and NIES, Japan	0.275	-0.529	0.237	25.6
2	MIROC-ESM-CHEM	JAMSTEC, AORI, and NIES, Japan	0.243	-0.491	0.233	25.2
3	MIROC5	JAMSTEC, AORI, and NIES, Japan	0.198	-0.183	-0.109	20.5
4	MPI-ESM-LR	Max Planck Institute for Meteorology, Germany	0.144	-0.133	-0.18	18.1
5	MPI-ESM-MR	Max Planck Institute for Meteorology, Germany	0.141	-0.093	-0.161	18.8
6	MPI-ESM-P	Max Planck Institute for Meteorology, Germany	0.126	-0.127	-0.165	18.5
7	MIROC4h	JAMSTEC, AORI, and NIES, Japan	0.124	-0.305	0.283	33.3
8	IPSL-CM5A-MR	Institut Pierre Simon Laplace (IPSL), France	0.087	-0.260	0.052	24.9
9	NorESM1-ME	Norwegian Climate Center	0.064	-0.095	0.156	24.2
10	GFDL-ESM2G	NOAA, GFDL, USA	0.060	-0.170	-0.009	24.6
11	GISS-E2-R	NASA / Goddard Institute for Space Studies, USA	0.059	0.016	0.162	22.0
12	CanESM2	CCCma, Canada	0.056	-0.126	0.006	29.5
13	ACCESS1-0	CSIRO, and Bureau of Meteorology, Australia	0.053	0.196	0.319	30.1
14	IPSL-CM5A-LR	Institut Pierre Simon Laplace (IPSL), France	0.051	-0.205	0.066	25.5
15	CNRM-CM5-2	CNRM and CERFACS, France	0.040	-0.037	0.057	25.3
16	CNRM-CM5	CNRM and CERFACS, France	0.035	-0.010	0.079	25.9
17	CESM1-FASTCHEM	DOE NCAR, USA	0.028	-0.053	-0.018	19.1
18	GFDL-ESM2M	NOAA GFDL, UISA	0.027	-0.086	0.017	24.1
19	NorESM1-M	Norwegian Climate Centre	0.025	-0.039	0.121	24.4
20	CCSM4	NCAR, USA	0.023	-0.034	-0.019	19.1
21	HadGEM2-ES	Met Office Hadley Centre, UK	0.012	0.240	0.069	26.6
22	CESM1-WACCM	DOE NCAR, USA	0.009	-0.082	-0.038	18.0
23	CESM1-BGC	DOE NCAR, USA	-0.001	-0.022	-0.050	18.5
24	GFDL-CM3	NOAA GFDL, USA	-0.034	0.142	-0.069	27.0
25	GISS-E2-H	NASA / Goddard Institute for Space Studies, USA	-0.037	0.158	-0.006	16.1
26	IPSL-CM5B-LR	Institut Pierre Simon Laplace (IPSL), France	-0.064	0.169	0.156	32.5
27	bcc-csm1-1	Beijing Climate Center (BCC), China	-0.083	0.105	0.096	19.3
28	inmcm4	Institute for Numerical Mathematics (INM), Russia	-0.090	0.130	0.019	25.6
29	bcc-csm1-1-m	Beijing Climate Center (BCC), China	-0.114	0.091	-0.061	23.3
30	MRI-ESM1	Meteorological Research Institute (MRI), Japan	-0.134	0.184	0.014	20.6
31	MRI-CGCM3	Meteorological Research Institute (MRI), Japan	-0.136	0.200	-0.007	19.8
	Ensemble mean		**0.040**	**-0.047**	**0.038**	**23.4**
	ERAI	ECMWF ERA-Interim reanalysis	0.185	-0.148	0.161	26.2